References

[1] Schooley, A. H. and Stewart, R. W., "Experiments with a Self-Propelled Body Submerged in a Fluid with a Vertical Density Gradient," *Journal of Fluid Mechanics,* Vol. 15, Pt. I, 1963, p. 83.

[2] Stockhausen, P. J., Clark, C. B., and Kennedy, J. F., "Three-Dimensional Momentumless Wakes in Density-Stratified Liquids," Rept. 93, 1966, MIT Hydrodynamics Lab., Cambridge, Mass.

[3] Prych, E. A., Harty, F. R., and Kennedy, J. F., "Turbulent Wakes in Density-Stratified Fluids of Finite Extent," TR 65, July 1964, Hydrodynamics Lab., MIT, Cambridge, Mass.

[4] Kennedy, J. F. and Froebel, R. A., "Two-Dimensional Turbulent Wakes in Density-Stratified Liquids," ASME Publication, 64-WA/UNT-11, 1964, New York.

[5] Van de Watering, W. P. M., "The Growth of a Turbulent Wake in a Density-Stratified Fluid," Rept. 231-12, 1966, Hydronautics, Inc., Laurel, Md.

[6] Van de Watering, W. P. M., Tulin, M. P., and Wu, J., "Experiments on Turbulent Wakes in a Stable Density-Stratified Environment," TR 231-24, 1969, Hydronautics, Inc., Laurel, Md.

[7] Schooley, A. H., "Wake Collapse in a Stratified Fluid," *Science,* Vol. 157, 1967, p. 421.

[8] Schooley, A. H., "Wake Collapse in a Stratified Fluid: Experimental Exploration of Scaling Characteristics," *Science,* Vol. 160, 1968, p. 763.

[9] Sundaram, T. R., Stratton, J., and Rehm, R. G., "Turbulent Wakes in a Stratified Medium," Rept. AG-3018-A-1, Nov. 1971, Calspan Corp., Buffalo, N.Y.

[10] Wu, J., "Collapse of Turbulent Wakes in Density Stratified Media," Rept. 231-4, 1965, Hydronautics, Inc., Laurel, Md.

[11] Wu, J., "Flow Phenomena Cause by the Collapse of a Mixed Region in a Density-Stratified Medium," Rept. 231-11, 1966, Hydronautics, Inc., Laurel, Md.

[12] Wu, J., "Wake Collapse and Subsequent Generation of Internal Waves in a Density-Stratified Medium," Rept. 231-17, 1968, Hydronautics, Inc., Laurel, Md.

[13] Wu, J., "Mixed Region Collapse with Internal Wave Generation in a Density-Stratified Medium," *Journal of Fluid Mechanics,* Vol. 35, Pt. 3, 1969, p. 531.

[14] Wessel, R., "A Numerical Study of the Collapse of a Perturbation in an Infinite, Density-Stratified Fluid," TR 169, 1968, Argonne National Lab., Argonne, Ill.; see also *Physics of Fluids,* Vol. 12, No. 12, 1969, II-171.

[15] Mei, C. C., "Collapse of a Homogeneous Fluid in a Stratified Fluid," *Proceedings of the 12th International Congress of Applied Mechanics,* edited by M. Hetenyi and W. G. Vincenti. Springer-Verlag, New York, 1969.

[16] Ko, D. R. S., "Collapse of a Turbulent Wake in a Stratified Medium," Rept. R-18202-6001-RO, Vol. 2, Nov. 1971, TRW Systems, Redondo Beach, Calif.

[17] Naudascher, E., "Flow in the Wake of Self-Propelled Bodies and Related Sources of Turbulence," *Journal of Fluid Mechanics,* Vol. 2, Pt. 4, 1965, p. 625.

[18] Pao, Y. H., "Turbulence Measurements in Stably Stratified Liquids," D1-82-0959, Feb. 1970, Boeing Scientific Research Lab., Seattle, Wash.

[19] Schooley, A. H. and Hughes, B. A., "An Experimental and Theoretical Study of Internal Waves Generated by the Collapse of a Two-Dimensional Mixed Region in a Density Gradient," *Journal of Fluid Mechanics,* Vol. 51, Pt. 1, 1972, pp. 159–175.

[20] Hartman, R. J. and Lewis, H. W., "Wake Collapse in a Stratified Fluid: Linear Treatment," *Journal of Fluid Mechanics,* Vol. 51, Pt. 3, 1972, pp. 613–618.

[21] Baker, D. J., "A Technique for Precise Measurement of Small Fluid Velocities," *Journal of Fluid Mechanics,* Vol. 26, 1966, p. 573.

[22] Merritt, G. E. and Rudinger, G., "Thermal and Momentum Diffusivity Measurements in a Turbulent Stratified Flow," AIAA Paper 72-80, San Diego, Calif., 1972.

[23] Birkhoff, G. and Zarantonello, E. H., *Jets, Wakes and Cavities,* Academic Press, New York, 1957.

JULY 1974 AIAA JOURNAL VOL. 12, NO. 7

Laminar Boundary Layer near the Symmetry Plane of a Prolate Spheroid

K. C. WANG*

Martin Marietta Laboratories, Baltimore, Md.

The previous investigation of a three-dimensional boundary layer near the plane of symmetry of an inclined spheroid has been extended to provide 1) wider range of solutions, 2) explanations to questions left unanswered before, and 3) comparisons with experiments. Extended solutions provide more complete trends of the boundary-layer behavior for incidences from 0°–90° and for thickness ratios ranging from unity for a sphere to nearly zero for a long inclined cylinder. Among these trends is how the separation changes from one type to another and then back again with increasing incidence. Explanations are given for a number of unconventional features, including the reversal of the lateral derivative of the cross velocity profile and the flattening of the longitudinal velocity profile. The latter has long been known as a two-dimensional turbulent boundary-layer phenomenon, and it is seen here also to be a three-dimensional phenomenon. Agreement with Wilson's recent experiments (designed specifically for partial check of the results obtained earlier) enhances the significance of the results.

Nomenclature

a = semimajor axis
A = regular boundary-layer region
b = semiminor axis
B = partially reversed region
C = separated region
c_f = skin friction
p = pressure
h_μ = metric coefficient
h_θ = metric coefficient
R = vortex starting point
Re = Reynolds number
S = separation point
u = meridional velocity
U = freestream meridional velocity
v = circumferential velocity
$\partial v/\partial\theta$ = circumferential derivative of v
$\partial V/\partial\theta$ = freestream $\partial v/\partial\theta$
z = normal coordinate
α = incidence angle
μ = meridional coordinate
θ = circumferential coordinate

Received May 17, 1973; revision received September 21, 1973. This research was sponsored by the Air Force Office of Scientific Research/AFSC, United States Air Force, under Contract 44620-70-C-0085.

Index category: Boundary Layers and Convective Heat Transfer—Laminar.

* Senior Research Scientist, Member AIAA.

1. Introduction

THE incompressible laminar boundary layer near the symmetry plane of an inclined body of revolution (a prolate spheroid) was exactly calculated by a finite-difference method in Ref. 1. Figure 1 shows the flow geometry. Profiles of u, $\partial v/\partial\theta$, and w were determined. The analysis introduced no restriction on the incidence or the thickness ratio beyond requiring that the pressure distribution be known. Several distinctive features were found, especially for the leeside boundary layer.

a) Reversal of $\partial v/\partial\theta$-Profile

As illustrated in Figs. 2a and 2b, a monotonic profile at an upstream point, gradually changes into a reversed profile at a downstream point Q. The change-over point, R, moves forward as the incidence increases. In contrast, reversal of the u-profile does not occur until a point, S, farther downstream, which is the separation point following the usual definition of separation. What is distinctive here is the existence of reversed profiles ahead of point S.

b) Flattening of u-Profile at Moderate-to-High Incidence

Instead of the profiles at successive downstream stations, 1–4, continuing to move up (Fig. 3a) as in low incidence as well as in familiar two-dimensional and axisymmetric cases, they first move up ($1 \rightarrow 2$) and then down ($2 \rightarrow 3 \rightarrow 4$), ending with a nearly flat profile (Fig. 3b). The flattening of velocity profile is used to be a two-dimensional turbulent boundary-layer phenomenon. Here we see that it is also a three-dimensional laminar phenomenon.

c) Forward and Rearward Movement of the Separation Point

As the incidence increases, the separation point S on the leeside does not move forward continuously; rather, it moves forward at low incidence and backward at higher incidence. This is in contrast to the usual concept, where the pressure gradient becomes more adverse as incidence increases, suggesting earlier flow separation.

Distinctive features also were noted in other results such as the skin friction and the displacement thickness, but these will not be discussed here. Some of these features were reported earlier in Ref. 1, and a preliminary discussion of the question of three-dimensional separation was presented. Since then, the problem has been elucidated gradually, and the implications of the earlier results on the concepts of separation were explored further by the author.[2] A surface-flow experiment by Stetson[3] was later found to be in clear agreement with the flow reversal, feature (a). Also, as a partial check of the calculations, experiments have been carried out by Wilson.[4] He investigated the leeside symmetry-plane boundary layer over a spheroid identical in geometry to that used in our calculation. The pressure and the u-velocity profiles at a number of stations were measured at various incidences. Smoke was injected from the rear to observe the separation point. The main findings, to be discussed later, agree with the foregoing cited features (b) and (c).

In the present work, we shall first in Sec. 2 attempt to clarify further the previously investigated incidence effects to the symmetry-plane boundary layer. This includes extension of the solutions to establish complete systematic trends of separation, further explanations of previously unexplained features, and comparisons with Wilson's experiment. Later in Sec. 3, we shall present results of the thickness effects on the symmetry-plane boundary layer over a spheroid at a fixed incidence. As the thickness ratio varies from unity to zero, the body shape changes from a sphere to a long cylinder, hence including a number of configurations of common interest. The central question for the latter investigation is how these aforementioned unconventional features will change if the thickness ratio varies. The present paper is based on a report[5] where more details can be found.

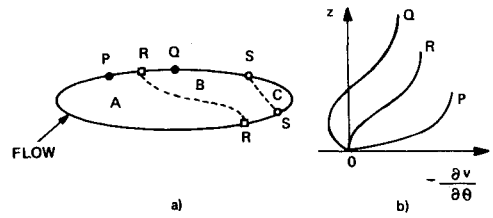

Fig. 2 Reversal of $\partial v/\partial\theta$-profile.

2. Incidence Effects

Predictability of the Cross-Flow Reversal

Among the unexplained unconventional features, one example is why and how the $\partial v/\partial\theta$-profile reverses. This reversal was found unexpectedly, but it can be predicted from the consideration of the sign change of the circumferential pressure curvature. Near the body surface ($z \rightarrow 0$), as the inertia terms drop out, Eq. (5c) in Ref. 1 becomes

$$\frac{\partial^2 p}{h_\theta \partial\theta^2} = \left[\frac{\partial^2}{\partial z^2}\left(\frac{\partial v}{\partial\theta}\right)\right]_{z\rightarrow 0}$$

which shows that the reversal of $\partial v/\partial\theta$-profile will occur only when the curvature $\partial^2 p/\partial\theta^2$ may become negative on the leeside and positive on the windside meridian. Results of $\partial^2 p/\partial\theta^2$ from the present extended calculation confirm that this is indeed the case.

The circumferential pressure curvature calculated maintains a consistent pattern with increasing incidence. In other words, it changes only in degree, but not in character with incidence. Consequently, flow features which depend strongly on this curvature follow a consistent trend. Such features include the variation of $\partial v/\partial\theta$-profile and the point at which $\partial v/\partial\theta$ reverses sign (i.e., point R, see Fig. 6).

Extended Calculations

The range of incidence in our earlier calculation[1] was from zero to 32°. This has now been extended to 90°. The new windside results continue to exhibit the trends established earlier,[1] but the new leeside results reveal additional significant features with respect to the separation phenomenon. We shall describe here only some highlights of the extended calculations to supplement what have already been reported in Ref. 1.

For the windside, as the incidence further increases from 30° to 90°, the pressure gradient continues to become favorable over most or all of the surface. The point of maximum pressure (i.e.,

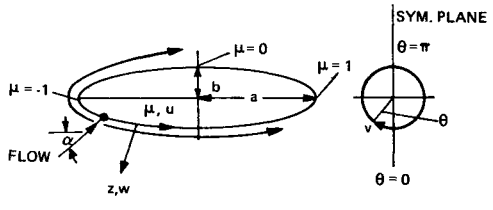

Fig. 1 Flow over a spheroid ($b/a = \frac{1}{4}$).

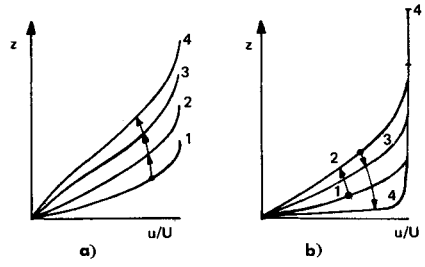

Fig. 3 Flattening of u-profile.

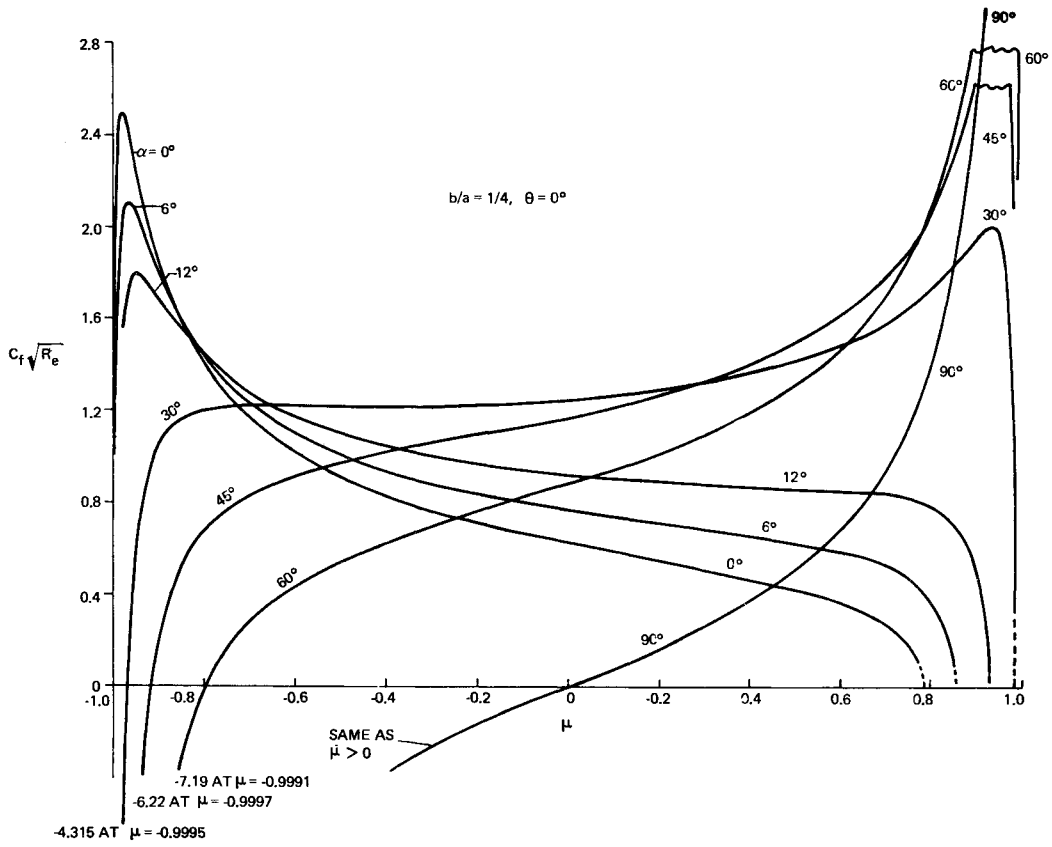

Fig. 4a Windside skin friction.

stagnation point) shifts very slowly downstream for incidences between 0° and 60°, (for $b/a = \frac{1}{4}$), but extremely rapidly for values between 60° and 90°. At a fixed μ-station, the μ-velocity profile becomes thinner; and from 45° incidence and up, it changes very little. At low incidences (0° ~ 12°), the u-velocity profile grows thicker in the downstream direction; at higher incidences (45° ~ 90°), this trend is reversed. In the intermediate range (say 30°), the u-velocity profile first grows thicker in the downstream direction, but stops growing and even becomes slightly thinner until shortly before separation. The $\partial v/\partial\theta$-profile behaves much the same as the u-profile. Such behavior of the basic profiles leads to the following results at higher incidences: the skin friction (Fig. 4a) continues to increase in the downstream direction (rather than decrease as in the low incidence cases), the separation point

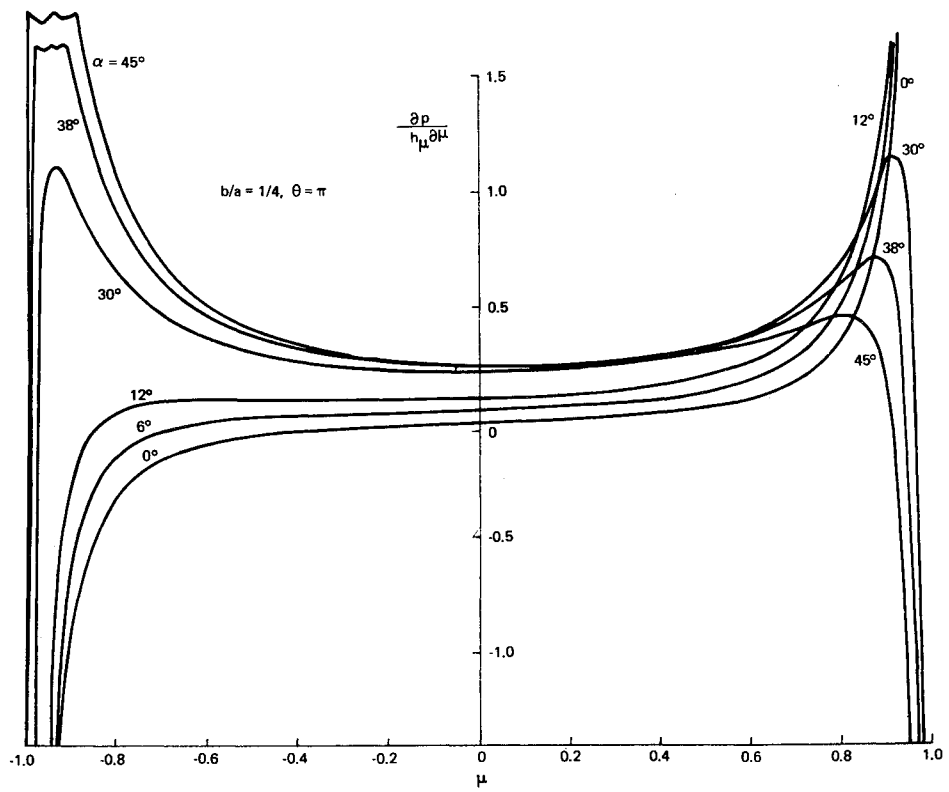

Fig. 4b Leeside meridional presure gradient.

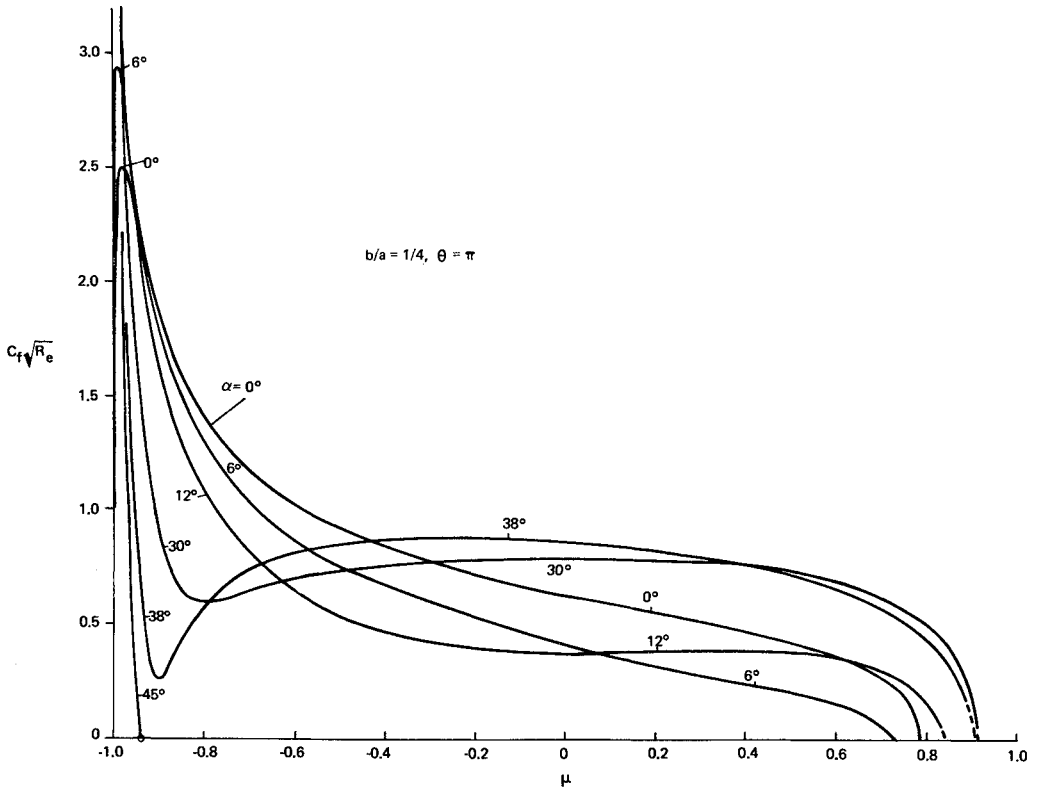

Fig. 4c Leeside skin friction.

continues to move downstream, and the displacement thickness becomes smaller at a fixed μ-station. At lower incidences ($0° \sim 12°$), the displacement thickness increases in the downstream direction; at the limiting high incidence (i.e., 90°), this trend is reversed. In the intermediate range, the displacement thickness first grows slowly and then shows little change or a slight decrease. The differences in the displacement thickness for incidences between 30° and 90° are very small. One is reminded that the displacement thickness referred to here is based on the u-velocity profile only. It presents an interesting contrast to the usual two-dimensional or axi-symmetrical case, but is not the complete displacement thickness in a three-dimensional flow involved here. This remark holds throughout this paper.

For the leeside, as the incidence increases, the meridional pressure gradient becomes more adverse, as expected. But what has usually not been noticed is how this gradient becomes more adverse (i.e., the effect of the meridional pressure curvature), and this turns out to have a great bearing on the leeside boundary-layer features. As shown in Fig. 4b, the meridional pressure gradient gradually becomes adverse for low incidences ($0° \sim 12°$), but at higher incidences it rises rapidly to a maximum in the front and then falls off. This leads to the formation of a "hump" or "barrier." Such behavior of the pressure gradient follows from the curvature change near the front in the pressure distribution (as shown in Fig. 7) case of 31.78° in Ref. 1. There, a large positive curvature changes quickly into a smaller negative one, implying precisely that an adverse pressure gradient rises rapidly to a maximum and then falls off thereafter.

When such a barrier is sufficiently high (e.g., 45° for $b/a = \frac{1}{4}$), the meridional flow near the surface would be stopped and separation occurs at the very front. When the "barrier" is not high enough and is therefore surmountable (say 30°, 38° cases), the flow may penetrate far back to the rear even after being severely decelerated. The resulting boundary-layer characteristics and the separation problem are quite altered (see later discussion on separation). The formation of a "barrier" of the meridional pressure gradient is also closely accompanied by a change of sign of circumferential pressure cirvature; hence the interplay between these two controlling factors over the symmetry-plane is evident.

Such meridional pressure gradient distribution gives rise to a number of unusual boundary-layer characteristics. These include, for example, the flattening of the u-velocity profile (which will be discussed later), the skin friction, and the movement of the separation point. The present extended calculation of skin friction at higher incidence brings out an important feature about separation. Although it was noted[1] that at low incidences, the skin friction (Fig. 4c) decreases from a maximum near the nose gradually and monotonically to zero at the separation points; at large incidence (say about 30°), the skin friction first drops rapidly to a minimum and increases gradually before it finally resumes its decline. Only after the calculation was extended to higher incidence, it became clear that this minimum grows deeper at larger incidence (38°), and finally the skin friction becomes zero near the front when the incidence is 40°. This result is important in developing a systematic separation picture. We shall return to this question later.

Comparisons with Wilson's Experiments

Wilson[4] carried out experiments to check specifically parts of the results calculated earlier. The experiment included measurements of the pressure, u-velocity profiles, and the separation point on the leeside of a spheroid with a thickness ratio of $\frac{1}{4}$.

Comparison of u-velocity profile

Presented in Figs. 5a and 5b are the u-velocity profiles at two leeside stations at different incidences. The experimental results

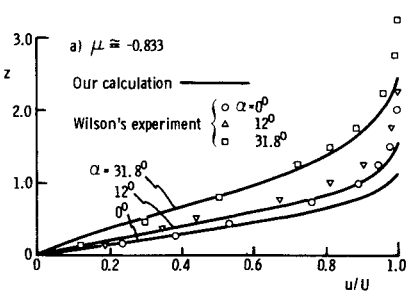

Fig. 5a Comparison of leeside u-velocity profile at $\mu = -0.833$.

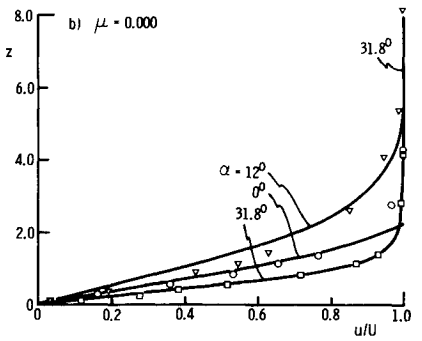

Fig. 5b Comparison of leeside u-velocity profile at $\mu = 0$.

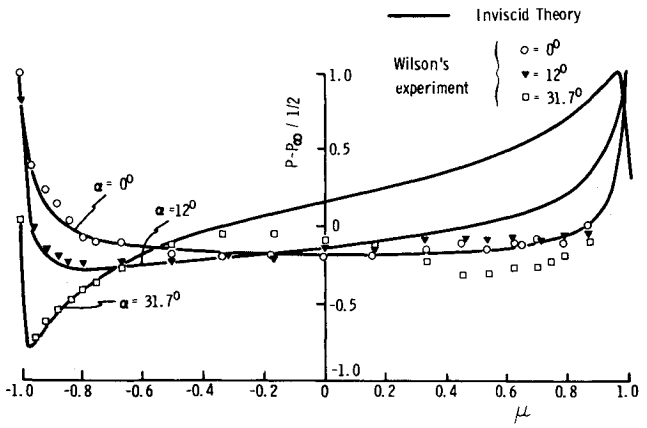

Fig. 5c Comparison of leeside pressure.

are taken directly from Wilson's thesis.[4] The agreement between theory and experiment is good. At an upstream station $\mu = -0.833$ (Fig. 5a), the profiles gradually move up (i.e., become thicker) as the incidence increases. The experimental boundary-layer thickness is somewhat greater than the calculated value. The relative position of these curves for different incidences is significant for our present purpose.

At the midstation, $\mu = 0$ (Fig. 5b), both the calculation and experiment indicate that the profiles for lower incidences including 0° grow thicker compared to their values in Fig. 5a; that for 12°, the profile grows only slightly thicker, whereas the 31.8° profile becomes much thinner and moves downward relative to those of 0° and 12°. In fact, it becomes thinner than the corresponding profile for the preceding station (Fig. 5a).

Comparisons at other stations generally show that for higher incidence, the profiles grow thinner at a faster rate according to the experiment. The most heartening fact resulting from these comparisons is Wilson's experimental confirmation of the theoretically predicted flattening trend of the u-profiles [feature (b) in Sec. 1].

Comparison of the separation point

Smoke visualization was used by Wilson to determine the separation point. Smoke was injected from the rear and the flow carried it forward until the point of separation was reached. Because of the limited precision of such a technique, the significance of smoke studies rests mostly with the qualitative indications of the relative movement of the separation point as the incidence changes. The following table gives the comparisons.

Table 1 Comparisons of separation point as incidence angle changes

Incidence (degrees)	Separation point (μ) Experiment	Calculation
0	0.61	0.7700
3	0.57	0.6600
6	0.68	0.7240
9	0.87	0.8070
12		0.8517

Both the experimental and calculated results display the same trend of the movement of the separation point, i.e., moving forward at low incidence and backward at higher incidence. Thus, Wilson's experiment supports the third feature (c) noted in Sec. 1.

Comparison of pressure distribution

Figure 5c, taken directly from Wilson's thesis, gives the comparison between experimental pressure and the pressure predicted by potential flow theory and used in our calculations. As

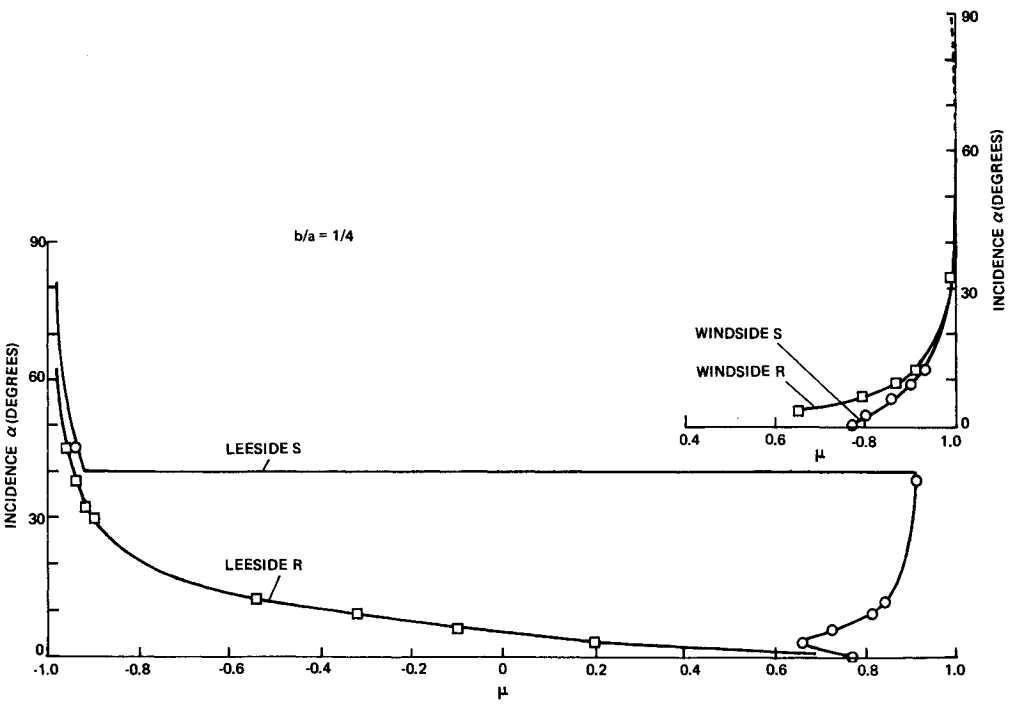

Fig. 6 Variation of points R and S with incidence.

expected, the agreement becomes poorer in the afterbody as the incidence increases. The rapid growth of the boundary-layer thickness on the leeside at high incidence makes the "actual" body fatter. The flow, therefore, becomes less decelerating and the pressure distribution becomes less adverse. Early measurements by Jones[6] show a similar trend.

Thus, it may be stated that Wilson's experiment confirms the new findings in our earlier work. We shall later comment on why the agreement between experiment and calculation is reasonably good, even at high incidence, despite the large difference in pressure distribution under these circumstances.

Systematic Separation Picture

Figure 6 summarizes the incidence effects on the location of the reversed flow starting point R and the separation point S. On the windside, both R and S gradually move rearward as the incidence increases. Movement is confined to a small distance near the rear. The leeside results are more complex and are important in the context of the general subject of three-dimensional laminar boundary-layer separation. As the incidence increases, point R moves continuously forward. On the other hand, point S first moves forward and later rearward, and then, at still higher incidence (approximately 40° for a spheroid of $b/a = \frac{1}{4}$), it jumps to the front end and moves slowly forward thereafter. Although the forward and rearward movement of the separation point near the rear end was noted earlier in Ref. 1 for incidences up to roughly 30°, and although, at extremely high incidence, one intuitively expects that the separation will occur on the forebody, it was not clear just how the transition actually takes place. Especially confusing was the aft shift of the separation point just prior to such a change.

The present result reveals that the change occurs in the form of a sudden jump rather than a gradual, smooth transition. This implies a sudden change of one type of separation (free vortex type) into another type (bubble type). The characteristics of these distinct types of separation have been discussed before.[2] In any case, the present leeside results provide a more complete separation picture for the whole range of incidence from zero to 90°.

Rearward Movement of the Leeside Separation Point

Another unconventional feature unexplained earlier[1] is the rearward movement of the leeside separation point. At high incidence, the pressure gradient becomes more adverse on the leeside but the separation point moves rearward instead of forward. At first glance, the validity of the prediction seems to be questionable.

In Wilson's experiment, the pressure gradient was found to be slightly favorable on the afterbody and this was interpreted as the cause of the rearward movement of the separation point. Although this interpretation appears to be reasonable, there is left unanswered the question of why the same behavior was first discovered in our earlier calculation where the theoretical pressure gradient was adverse. There is no doubt that favorable or less adverse pressure gradient in the afterbody on the leeside would tend to move the separation point rearward; but this is not the main reason, because the same phenomenon occurs also in an environment of adverse pressure gradient.

A more direct cause for the rearward movement may be the flattening of the u-velocity profile. A flat near-uniform velocity profile certainly carries larger momentum and, hence, can penetrate the adverse pressure gradient farther so that the separation is postponed. Since the flattening of the u-velocity profile was found in both Wilson's experiment and our calculations, this interpretation is consistent with both observations.

One may then wonder how the flattening of the u-velocity profile happens, especially where the pressure gradient is adverse. Two-dimensional boundary-layer theory normally dictates that an adverse pressure gradient tends to steepen the profile rather than to flatten it, but this rule is not followed in the present three-dimensional case. Here, the flattening of the u-velocity profile results from the decrease of meridional pressure gradient behind a peak and from the reversal of the $\partial v/\partial\theta$-profile near the surface. Intuitively, it seems that when the fluid near the surface flows away from (rather than toward) the symmetry plane, the symmetry plane flow (again near the surface) will be accelerated, so that the profile across the boundary layer will become more uniform.

Validity of the Leeside Solution at High Incidence

In our first calculation,[1] we noted that, since the boundary-layer thickness is so large, 1) the basic concepts for a thin boundary layer may no longer hold, and 2) the theoretical pressure is bound to be inaccurate. These considerations are further augmented by the unconventional nature of the results obtained and raise a question of the validity of those results.

Later in Ref. 2, it was suggested that flow in the leeside region under the circumstances considered is indeed in an unconventional "separated" state. By "unconventional" it is meant here that 1) the separated region originates from the same front stagnation point, as does the unseparated region, and 2) the separation line does not pass through singular points of the limiting streamlines.

We contend that the leeside symmetry-plane boundary layer can be calculated up to the point S; the results check well in the front portion and agree at least qualitatively in the after-portion with Wilson's experiment. We take this as evidence in supporting our calculated solutions. It is true that this meridional pressure distribution is seriously inaccurate on the afterbody, but the symmetry-plane flow is not determined by this pressure gradient alone. In fact, the circumferential pressure curvature for a body of revolution, as shown before, changes for all cases only in degree but not in character. This property will persist to a large extent even when the change in body shape due to the boundary-layer thickness is taken into account; the resulting cross section will still be a smooth symmetrical one.

3. Thickness Effects

Previous investigations of the thickness effects on the boundary layer over elliptical cylinders and spheroids have been presented by Pretsch[7] and Schlichting[8] for zero incidence using the momentum integral method. Here, we consider the thickness effects (Fig. 7) on the symmetry-plane boundary layer at a fixed moderate incidence. We shall see that a change of thickness affects the windside and the leeside symmetry-plane boundary layers in rather different ways and that, if the axisymmetric case were chosen to study the thickness effects, one then would obtain a picture similar to that for the windside only while other more interesting features on the leeside will not be uncovered.

Windside Results

Figure 8a gives the windside pressure distribution. As the thickness ratio decreases, this distribution generally becomes linear (except near the ends), and its magnitude becomes rather small. The distribution changes from one which is favorable at the front and adverse at the rear to one slightly favorable throughout most of the windside.

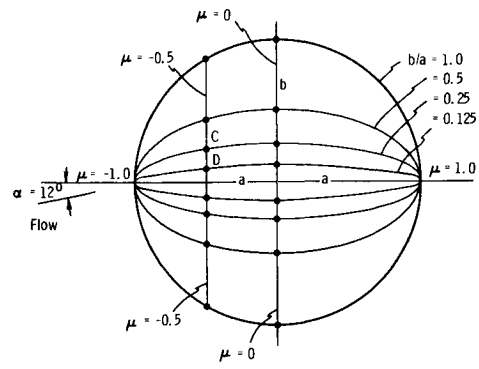

Fig. 7 Spheroid of different thickness ratios.

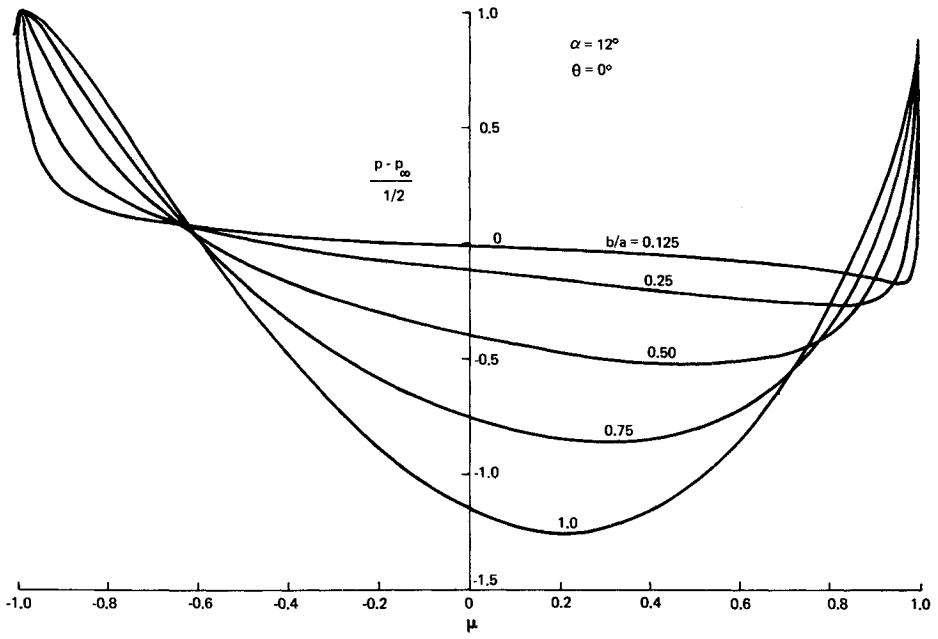

Fig. 8a Windside pressure.

As the thickness ratio decreases, the circumferential pressure curvature (Fig. 8b) increases in magnitude, and the point where its sign changes from positive to negative moves aft. Change of thickness merely shifts the distribution curve downward with little change in character. This property also was noted in connection with the incidence effects. So far as this pressure curvature is concerned, a decrease in thickness ratio at a fixed incidence has an effect similar to that of an increase in incidence for a fixed body. Hence, flow features mainly influenced by this pressure curvature will be expected to exhibit the same trend.

At a fixed μ-station, the u-profile generally becomes thinner as the thickness decreases, and this pattern is maintained throughout the windside. For fixed higher thickness ratios (say, $b/a > 0.5$), the profile continues to grow thicker in the downstream direction (i.e., steepen up as depicted in Fig. 3a); whereas for fixed lower thickness ratios (say $b/a = 0.125$), the profile grows only a little thicker in the front and remains almost unchanged thereafter. It is noted that decrease of thickness at fixed incidence and increase of incidence for fixed body also have generally similar effects on the windside u-velocity profile even though the meridional pressure gradient behaves quite differently in the two cases.

The $\partial v/\partial\theta$-profile behaves very much the same as the u-velocity profile just described. A reversed shape appears only a short distance ahead of the separation near the rear end for higher thickness ratios. The point, R, where the reversed profile starts, is shown later in Fig. 10 together with the separation point.

Figure 8c gives the skin friction along the windside symmetry plane. As the thickness decreases, the skin friction generally becomes larger and the separation point gradually moves downstream.

Figure 8d gives the displacement thickness distribution. With decrease of the thickness ratio, the displacement thickness decreases as the skin friction increases. For fixed larger thickness ratios ($b/a > 0.25$), $\Delta_\mu{}^*$ remains nearly constant. Figure 8d bears a strong resemblance to Fig. 6f of Ref. 1, with the correspondence between decrease in thickness ratios and increase in incidence.

Leeside Results

The leeside pressure distribution can be seen from Fig. 8a by a reflection about the vertical axis. For example, in the case of $b/a = 0.125$, the pressure distribution will become slightly adverse

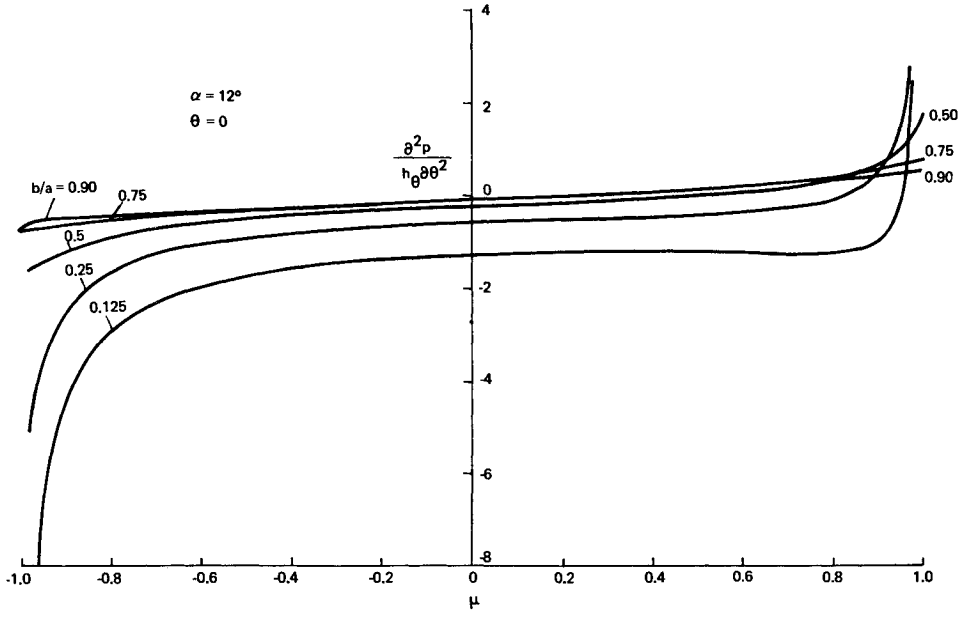

Fig. 8b Windside circumferential pressure curvature.

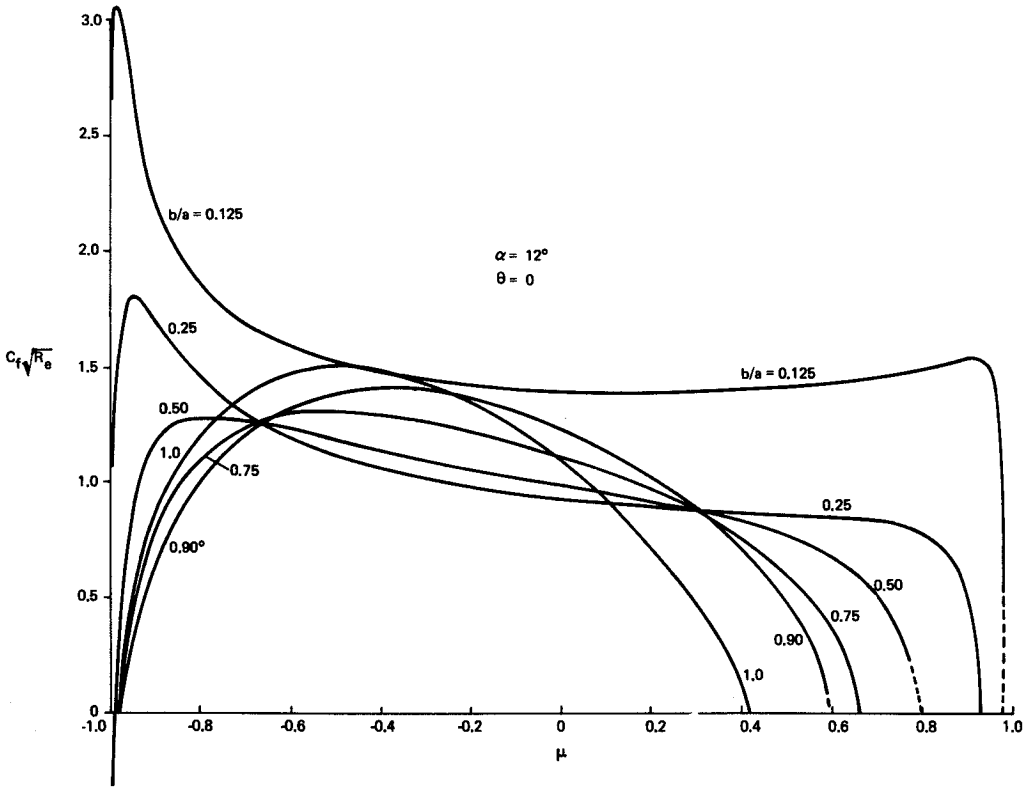

Fig. 8c Windside skin friction.

(rather than favorable as on the windside) throughout most of the leeside. The leeside circumferential pressure curvature can be similarly seen from Fig. 8b.

On the leeside, the boundary layer is always much thicker and also more complex. At a fixed front μ-station, the u-profile becomes thinner as the thickness ratio decreases. This pattern is the same as on the windside. However unlike in the windside case, this pattern is not maintained at fixed downstream stations. This results from the fact that u-profile grows faster over more slender (smaller thickness ratio) shapes at a fixed incidence. The latter, in turn, reflects the fact that a more slender shape is more sensitive to the incidence effect. Consequently, at downstream stations, the u-profile for smaller thickness ratios may become thicker (rather than thinner as on the windside) than that for larger thickness ratios.

Furthermore, the leeside u-profile for a given larger thickness ratio at fixed incidence continues to steepen up in the downstream stations (as the pattern depicted in Fig. 3a); but that for a smaller thickness ratio first steepens up and then flattens down, corresponding to the pattern depicted in Fig. 3b. This, again, suggests a correspondence between the decrease of thickness ratio at a fixed incidence and the increase of incidence for a fixed body.

The $\partial v/\partial\theta$-profile on the leeside differs from the u-profile mainly in the occurrence of flow reversal. The earlier the reversal of $\partial v/\partial\theta$-profile starts, the smaller is the thickness ratio. The correspondence between increase of incidences for a fixed body and

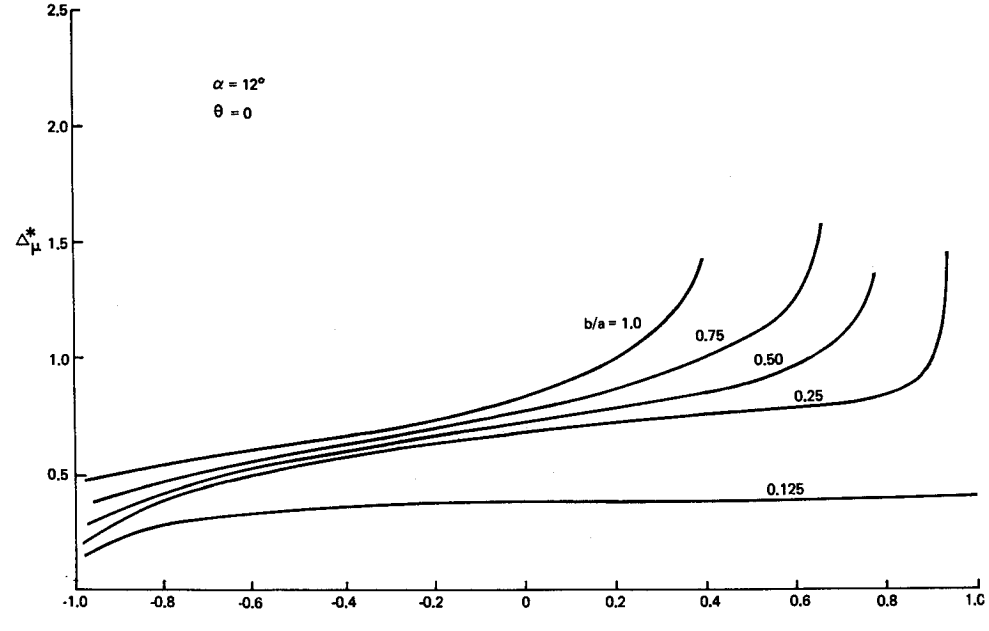

Fig. 8d Windside displacement thickness.

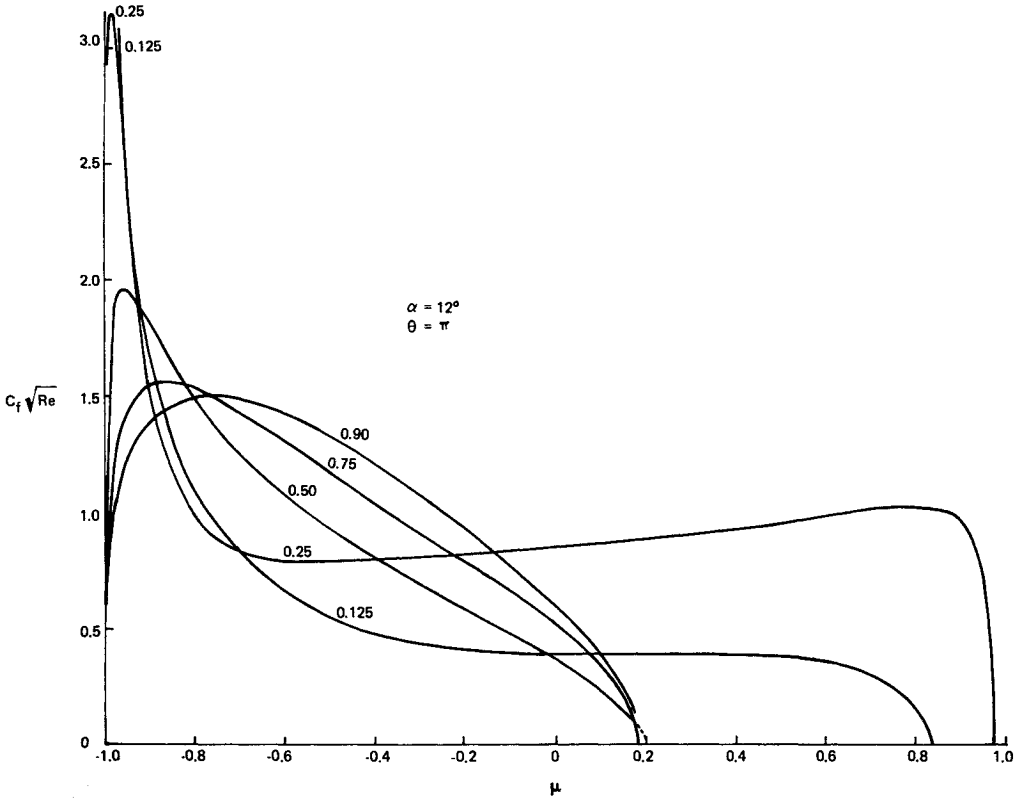

Fig. 9a Leeside skin friction.

decrease of thickness ratios at a fixed incidence is noted to be even more complete in the $\partial v/\partial\theta$-profiles. This is apparently due to the correspondence in their respective circumferential pressure curvature distributions, as pointed out before.

Figure 9a presents the skin-friction distributions on the leeside. It displays clearly the gradual change from the familiar half-oval shape distribution for a sphere to the distribution for a long cylinder. Compared to Fig. 8c for the windside, the leeside skin friction for smaller thickness ratios becomes smaller (rather than larger, as in the windside), because the pressure is less adverse.

Figure 9b gives the displacement thickness distribution on the leeside. For larger thickness ratios, the displacement thickness increases continuously in the downstream direction, whereas for smaller thickness ratios, it increases first and then falls off. This follows from the fact that the u-velocity profiles continue to grow thicker in the former, but the u-profiles grow thicker first and then thinner in the latter. A close resemblance between the present Fig. 9b and Fig. 7f of our earlier work[1] is noted, and there is a definite correspondence between increase in incidence and decrease in thickness ratio.

Conclusions

In several aspects, it is seen that decreasing the thickness at a fixed incidence has an effect similar to that of increasing the incidence for a fixed body.

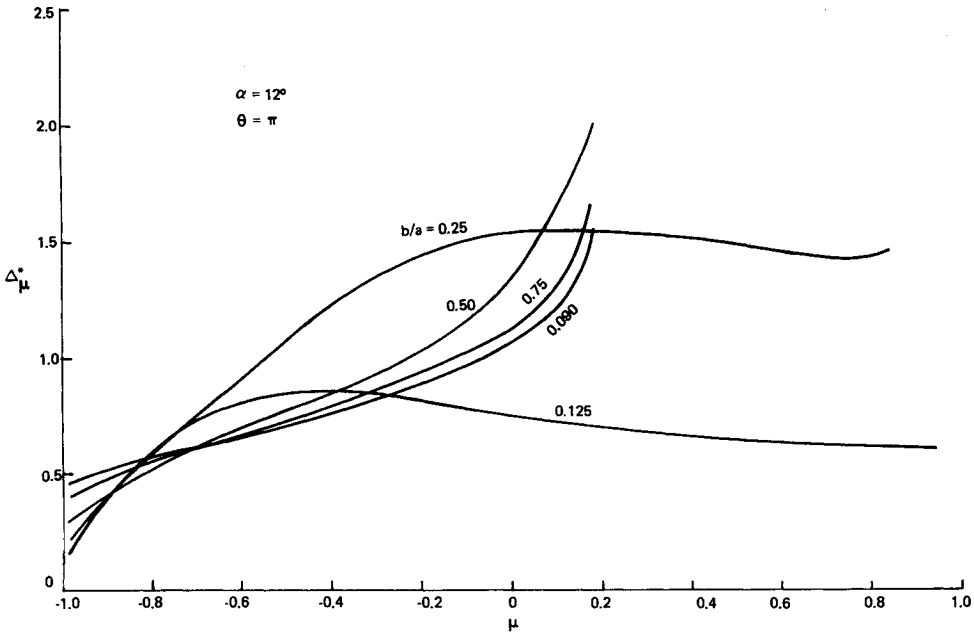

Fig. 9b Leeside displacement thickness.

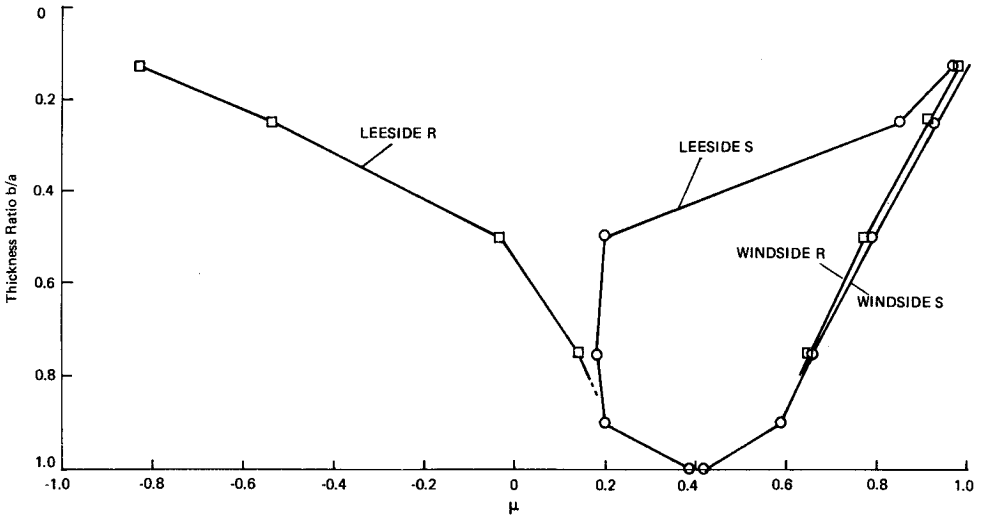

Fig. 10 Variation of R and S with thickness.

The systematic variation of the thickness effects on the location of the reversed flow starting point R and the separation point S is summed up in Fig. 10. On the windside, both R and S gradually move rearward as the thickness decreases. On the leeside, while point R moves continuously forward, point S moves first forward and then rearward. It is very likely that point S would jump to the front end as the thickness continues to decrease in analog to the same jump shown in Fig. 6. Compared to Fig. 6, the aforementioned correspondence between decreasing the thickness at a fixed incidence and increasing the incidence for a fixed body generally prevails.

In response to our opening question in the Introduction, namely, how features of the incidence effects will change if the thickness changes, we would like to conclude by reiterating the following two points: 1) these features, and especially the separation phenomena regarding points R and S for a fixed body at different incidences, prevail for other bodies also; and 2) the incidence effects are more pronounced for a more slender body. The leeside symmetry-plane boundary layer of b/a equal to 0.125 at 12° incidence has all the characteristics of the boundary layer associated with a b/a equal to 0.25 at incidence slightly below 30°. The abrupt change in type of separation that occurs for b/a equal to 0.25 at about 40° incidence may be assumed to take place at considerably lower incidence for b/a equal to 0.125.

References

[1] Wang, K. C., "Three-Dimensional Boundary Layer Near the Plane of Symmetry of a Spheroid at Incidence," *Journal of Fluid Mechanics*, Vol. 43, Pt. 1, Aug. 1970, pp. 187–209.

[2] Wang, K. C., "Separation Patterns of Boundary Layer over an Inclined Body of Revolution," *AIAA Journal*, Vol. 10, No. 8, Aug. 1972, pp. 1044–1050.

[3] Stetson, K. F., "Boundary-Layer Separation on Slender Cones at Angle of Attack," *AIAA Journal*, Vol. 10, No. 5, May 1972, pp. 642–648.

[4] Wilson, G. R., "Experimental Study of Laminar Boundary Layer on a Body of Revolution," Master's thesis GAM/AE/71-4, March 1971, Air Force Inst. of Technology, Wright-Patterson Air Force Base, Ohio.

[5] Wang, K. C., "Further Investigation of Three-Dimensional Boundary Layer Near the Symmetry Plane of an Inclined Body of Revolution," TR71-14C, Sept. 1971, RIAS, Martin Marietta Corp., Baltimore, Md.

[6] Jones, R., "The Distribution of Normal Pressures on a Prolate Spheroid," ARC R & M 1061, 1927, Aeronautical Research Council, London, England.

[7] Pretsch, J., "Die Laminare Reibungschicht an Elliptischen Zylimdern Und Rotationsellipsoiden bei Symmetrischer Anströmung," *Luftfahrtforschung*, Vol. 18, 1941, p. 397.

[8] Schlichting, H., *Boundary Layer Theory*, 4th ed., McGraw-Hill, New York, 1960.